Stem Cell Reports
Resource
OPEN ACCESS

Integrated Analysis of Contractile Kinetics, Force Generation, and Electrical Activity in Single Human Stem Cell-Derived Cardiomyocytes

Jan David Kijlstra,[1,2,3,9] Dongjian Hu,[1,2,4,9] Nikhil Mittal,[5] Eduardo Kausel,[6] Peter van der Meer,[3] Arman Garakani,[7] and Ibrahim J. Domian[1,2,8,*]

[1]Cardiovascular Research Center, Massachusetts General Hospital, Boston, MA 02114, USA
[2]Harvard Medical School, Boston, MA 02115, USA
[3]University Medical Center Groningen, University of Groningen, Groningen, 9713 GZ, the Netherlands
[4]Department of Biomedical Engineering, Boston University, Boston, MA 02215, USA
[5]Institute of Bioengineering and Nanotechnology, 138669 Singapore
[6]Department of Civil and Environmental Engineering, Massachusetts Institute of Technology, Cambridge, MA 02139, USA
[7]Reify Corporation, Saratoga, CA 95070, USA
[8]Harvard Stem Cell Institute, Cambridge, MA 02138, USA
[9]Co-first author
*Correspondence: domian@mgh.harvard.edu
http://dx.doi.org/10.1016/j.stemcr.2015.10.017

SUMMARY

The quantitative analysis of cardiomyocyte function is essential for stem cell-based approaches for the in vitro study of human cardiac physiology and pathophysiology. We present a method to comprehensively assess the function of single human pluripotent stem cell-derived cardiomyocyte (hPSC-CMs) through simultaneous quantitative analysis of contraction kinetics, force generation, and electrical activity. We demonstrate that statistical analysis of movies of contracting hPSC-CMs can be used to quantify changes in cellular morphology over time and compute contractile kinetics. Using a biomechanical model that incorporates substrate stiffness, we calculate cardiomyocyte force generation at single-cell resolution and validate this approach with conventional traction force microscopy. The addition of fluorescent calcium indicators or membrane potential dyes allows the simultaneous analysis of contractility and calcium handling or action potential morphology. Accordingly, our approach has the potential for broad application in the study of cardiac disease, drug discovery, and cardiotoxicity screening.

INTRODUCTION

Advanced heart failure represents a leading cause of mortality and morbidity in the developed world. The clinical syndrome results from an inability of the cardiac output to meet the metabolic demands of affected individuals. Most commonly, this results from a loss of myocardial cell viability or function (de Tombe, 1998; Narula et al., 1998). Cardiomyocytes (CMs), the basic functional units of the myocardium, produce force by shortening and thickening during each contractile cycle to generate the forward flow of blood. In vitro, myocardial function has been studied at the single-cell level or by myocardial muscle constructs as a surrogate for in vivo myocardium (Zimmermann et al., 2006). The use of adult CMs isolated from the myocardium of adult rodents and other animals for in vitro studies of cardiac physiology and pathophysiology has been an established method since the 1970s (Glick et al., 1974). As a result, most techniques used to quantify the contractility of CMs have been optimized for cells with distinct edges and highly developed sarcomeres.

Recent advances in stem cell biology have greatly increased the efficiency of cardiac differentiation of human pluripotent stem cells (Lian et al., 2012). Human pluripotent stem cell-derived cardiomyocytes (hPSC-CMs) are now used widely for in vitro studies (Sun et al., 2012) and as cell sources for regenerative cardiovascular medicine (Chong et al., 2014; Zimmermann et al., 2006). However, hPSC-CMs display a relatively less mature phenotype and often lack distinct cell edges and highly developed sarcomeres, making the study of their contractility with traditional techniques difficult. This has prompted a number of laboratories to focus on the functional maturation of stem cell-derived CMs (Yang et al., 2014). Although progress has been made in this regard, the goal of culturing fully mature human CMs from hPSC-CMs remains elusive, highlighting the need for novel methods to functionally characterize CMs at different developmental states.

Two widely used methods to quantify the contractile kinetics of adult CMs are edge detection and sarcomere length measurements (Bub et al., 2010; Chen et al., 2014). Edge detection technology relies on automatically detecting changes in the position of the longitudinal edges of a CM over time. Accordingly, its application must be optimized for the scale, clarity, and orientation of the images being analyzed. Commercially available edge detection tools used to study CMs, for example, have been optimized to detect the outer edges of horizontally aligned isolated adult rod-like CMs that are either in suspension or attached to glass (Chen et al., 2014). These tools are therefore not ideal

for the assessment of hPSC-CMs with indistinct borders. Moreover, glass is not an ideal substrate for CMs when studying their contraction kinetics because the stiffness of glass far exceeds the force generated by contracting CMs. Alternative approaches for the quantification of contractility of adult CMs include assessment of the change of sarcomere length over time. This approach requires the presence of distinct sarcomeres (Bub et al., 2010) and is therefore not very well suited for the study of hPSC-CMs.

Several approaches have been described recently for analyzing motion in movies of beating hPSC-CMs, collectively referred to as optical flow analysis. These approaches include motion vector analysis after manual segmentation (Ahola et al., 2014), block-matching algorithms combined with motion vector analysis (Hayakawa et al., 2014), or the evaluation of the correlation between intensity vectors of frames within a movie (Maddah et al., 2015) to yield a unit-less or dual-peaked curve representing the beating signal. These approaches, however, do not directly allow for the quantitative assessment of fractional shortening and force generation kinetics, key features of cardiomyocyte physiology. CM force generation has been assessed previously by a number of different methods, including fluorescent microsphere-based traction force microscopy, atomic force microscopy, and micropost deformation measurements (Liu et al., 2012; McCain et al., 2014; Rodriguez et al., 2014). These techniques are highly specialized, require advanced instrumentation, and cannot be easily combined with optical measurements of contractile kinetics, measurements of calcium cycling, or action potentials.

Here we present a methodology for the quantitative analysis of CM contractile kinetics and force generation that can be used in hPSC-CMs as well as isolated adult CMs. Our approach is not based on tracking the motion of parts of the cell but, rather, on quantifying the total amount of change in cell morphology over time. We use a previously well validated statistical tool to analyze the similarity between frames in movies of contracting human embryonic stem cell-derived cardiomyocytes (hESC-CMs) to generate a similarity matrix. This matrix represents the change in cell morphology over time and is used to compute the contractile kinetics of hESC-CMs. We combine this methodology with a biomechanical model to concurrently calculate the CM force generation as the CMs deform a flexible substrate. We validate this approach in human stem cell-derived CMs as well as in murine adult myocardial cells at single-cell resolution as well as in myocardial clusters. We further demonstrate our ability to detect subtle changes in the contractile kinetics and force generation of hESC-CMs in response to pharmacological intervention with isoproterenol and verapamil. Furthermore, we show that our methodology can be applied simultaneously with other single-cell physiological assays for the quantification of calcium cycling and action potentials. Finally, we show the utility of this method in assessing the cardiotoxicity of drugs such as dofetilide.

RESULTS

Morphologic Similarity Measure to Produce Contraction Curves

The goal of this study is to generate a high-throughput unbiased and robust methodology for the analysis of contraction kinetics and force generation of stem cell-derived CMs that is compatible with fluorescence-based calcium cycling and action potential assessment. We therefore performed directed differentiation to generate hESC-CMs. On days 13–20 of in vitro differentiation, CMs were dissociated into single-cell suspension and plated on a polydimethylsiloxane (PDMS) flexible substrate at single-cell density. By culturing these CMs on the PDMS flexible substrate, the cells could contract against strain (McCain et al., 2014). After 14 days of culture on the flexible substrate, cells were visualized in a temperature- and CO_2-controlled chamber by differential interference contrast (DIC) imaging as described in the Experimental Procedures. We acquired movies of the contracting cells at a temporal resolution of at least 100 frames/s (fps).

As an example to illustrate our methodology, a 300-frame movie at 100 fps of a single hESC-derived rod-like CM undergoing a single contraction cycle was analyzed (Movie S1). As shown, the CM of Movie S1 is in a pre-contractile relaxed state between frames 1 (F1) and F140 and shortens between F140 and F165 before returning to the baseline-relaxed state. We first sought to determine the change in cell morphology during these 300 frames. We therefore quantitatively assessed the similarity of F1 to every other frame in the movie by performing a pairwise similarity comparison (SC) using a well established statistical tool (Figure 1A; Garakani et al., 2015; Drubin et al., 2006; Garakani, 2008; Hack et al., 2004; C.A. MacRae et al., 2005, International Conference on Systems Biology, conference presentation). This equation calculates the SC for all pairs of frames captured at times i and j ($i \neq j$). Each pair of frames is compared based on the color intensity of spatially corresponding pixels defined by an intensity function $I_{x,y,t'}$, where x and y are integers defining the coordinates of a given pixel in a particular frame and t′ is an integer corresponding to the time of capture of the frame. The intensity function values of all pixels in each frame are summated over N, where N is the total width × total height of each frame. The similarity function is commutative so that $SC_{i,j} = SC_{j,i}$. Furthermore, $SC_{i,j} = 1$ if $i = j$. Therefore, SC is defined as having a value between 0 and 1 where,

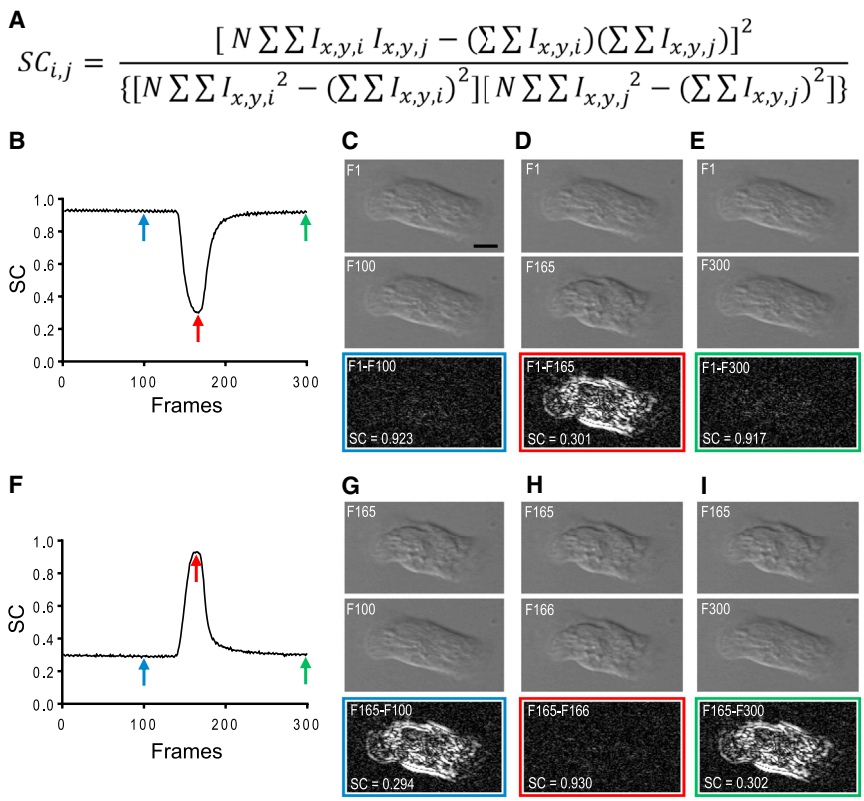

Figure 1. Pairwise Similarity Comparison of Frames in a Movie of a Contracting CM

(A) The equation to calculate SC between two frames. Each pair of frames is compared based on the intensity (grayscale value) of pixels in the same location of the two frames. The intensity is defined by the function $I_{x,y,i}$, where x and y define the coordinates of a given pixel in frame *i*. The values of all pixels in each frame are summed over the frame area (N). The similarity function is commutative so that $SC_{i,j} = SC_{j,I}$. The SC of two identical frames is defined as 1.

(B) A plot of SCs of frame F1 versus every other frame of Movie S1. Blue, red, and green arrows refer to the SCs for F1 versus F100, F165, and F300, respectively.

(C) The digital difference between the relaxed frame F1 (top) and the pre-contractile frame F100 (center) is displayed at the bottom with the associated SC value.

(D) The digital difference between F1 (top) and the contractile frame F165 (center) is displayed at the bottom with the associated SC value.

(E) The digital difference between F1 (top) and the post-contractile frame F300 (center) is displayed at the bottom with the associated SC value.

Scale bar, 10 μm. See also Movie S1.

the more similar two frames are to each other, the closer their SC value is to 1. We plotted the pairwise SC value of F1 against every other frame, which yielded a preliminary analysis of the contraction cycle (Figure 1B). The SC of the relaxed frame F1 versus the pre-contractile frames F2–F140 resulted in relatively high SC values (highly similar). The SC values of F1 versus the contractile frames (F141–F165) dropped dramatically (highly dissimilar). And, finally, the SC values of F1 versus the post-contractile frames returned to the high baseline value (again highly similar).

To visually display the outcome of the SC analysis, we used Fiji to calculate the digital differences between F1 and the pre-contractile frame F100. Spatially corresponding pixels that have a similar intensity result in a dark pixel, and corresponding pixels that have a less similar intensity result in a lighter pixel. This calculation resulted in an essentially black image with a faint, apparently random white-speckled background and an associated SC of 0.923 because these two frames are both acquired while the cell is in a relaxed state and very similar, although not identical. (Figure 1C). The digital difference of F1 and the contractile frame F165 resulted in a high-contrast black-and-white image with an associated SC of 0.301, indicating a clear signal because the change in cell morphology has resulted in a change of the intensity of many pixels compared with the corresponding pixels in the other frame (Figure 1D). Finally, the digital difference between F1 and the post-contractile frame F300 again yielded an essentially black image with a faint white-speckled background and an associated SC of 0.917 (Figure 1E).

In contrast, pairwise analysis of contractile frame F165 to every other frame resulted in an inverted-appearing contractile cycle (Figure 1F). The SC value of F165 versus the relaxed frames was very low (highly dissimilar), became progressively higher (more similar) for the contractile frames, and dropped again for the post-contractile frames. Likewise, the digital difference of F165 versus the pre-contractile frame F100 was a high-contrast image with an associated SC of 0.294 (Figure 1G). The digital difference of F165 versus the contractile frame F166 was essentially black with a faint white-speckled background and an associated SC of 0.930 (Figure 1H). And, finally, the digital difference of F165 versus the post-contractile frame F300 was again a high-contrast black-and-white image with an associated SC value of 0.302 (Figure 1I).

To capture all of the similarity data in the movie, we performed a pairwise comparison of each frame in Movie S1

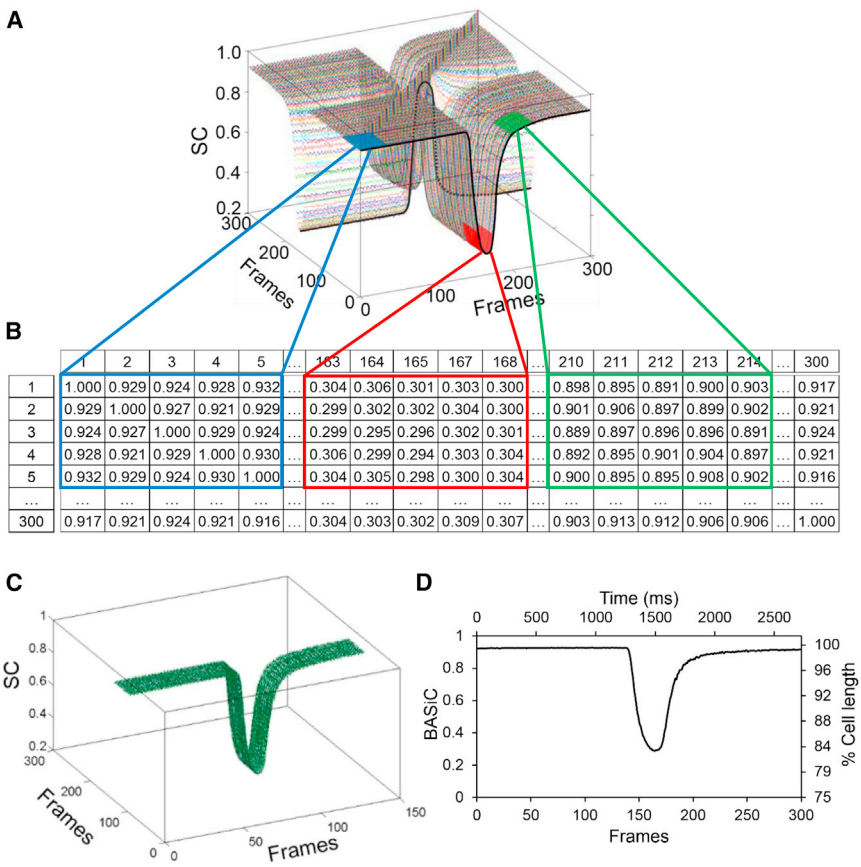

	1	2	3	4	5	…	163	164	165	167	168	…	210	211	212	213	214	…	300
1	1.000	0.929	0.924	0.928	0.932	…	0.304	0.306	0.301	0.303	0.300	…	0.898	0.895	0.891	0.900	0.903	…	0.917
2	0.929	1.000	0.927	0.921	0.929	…	0.299	0.302	0.302	0.304	0.300	…	0.901	0.906	0.897	0.899	0.902	…	0.921
3	0.924	0.927	1.000	0.929	0.924	…	0.299	0.295	0.296	0.302	0.301	…	0.889	0.897	0.896	0.896	0.891	…	0.924
4	0.928	0.921	0.929	1.000	0.930	…	0.306	0.299	0.294	0.303	0.304	…	0.892	0.895	0.901	0.904	0.897	…	0.921
5	0.932	0.929	0.924	0.930	1.000	…	0.304	0.305	0.298	0.300	0.304	…	0.900	0.895	0.895	0.908	0.902	…	0.916
…	…	…	…	…	…	…	…	…	…	…	…	…	…	…	…	…	…	…	…
300	0.917	0.921	0.924	0.921	0.916	…	0.304	0.303	0.302	0.309	0.307	…	0.903	0.913	0.912	0.906	0.906	…	1.000

Figure 2. Generation of the Contraction Curve from the Similarity Matrix

(A and B) Three-dimensional graph (A) displaying the similarity matrix (B) of Movie S1, where the x and y axes display frame numbers and the z axis displays the SC value. The highlighted black lines display the SC plots of F1 and F165 versus every other frame. The blue, red, and green planes map areas of the three-dimensional graph to the associated portion of the matrix.

(C) Three-dimensional graph of the selected pre-contractile SC curves.

(D) BASiC normalized to cell length and time for the generation of a standard contraction curve.

See also Figure S1 and Table S1.

versus every other frame to produce a similarity matrix of 300 rows × 300 columns, where each row of the matrix contains a series of SCs for a specific frame versus every other frame (Table S1). The 300 × 300 similarity matrix was then plotted as a series of similarity curves in a three-dimensional graph (Figure 2A). Sample portions of the 300 × 300 matrix are displayed (Figure 2B), with the left showing the pairwise comparison of pre-contractile frames F1–F5 versus F1–F5 (all highly similar), the center showing F1–F5 versus contractile frames F163–F168 (highly dissimilar), and the right showing F1–F5 versus post-contractile frames F210–214 (all highly similar again).

To obtain a more physiological assessment of the CM contraction cycle, we used the average of the similarity curves of pre-contractile frames (Figure 2C) as the baseline for the maximally relaxed state. We defined the pre-contractile period as the terminal 15% of the inter-contraction interval, as determined by a rolling linear regression analysis of all frames (Figures S1A and S1B). Next we averaged these similarity curves to obtain the baseline adjusted similarity comparison (BASiC) curve. We then normalized the maximum and minimum SC values to manually measured cell length at end-diastole and peak systole (as described in detail in the Supplemental Experimental Procedures). This allowed us to generate a normalized contraction curve of CMs with percent cell length plotted against time (Figure 2D). Manually measured cell length measurements were highly similar between independent observers, with a mean difference of 0.3 μm (95% limit of agreement, −1.8–1.2 μm; Figure S1C).

We then empirically validated this quantitative analysis and demonstrated that the BASiC-generated cell length curves correlate with contraction curves generated by manual cell length measurement, automated edge detection measurement, and sarcomere length measurement with Pearson's correlation coefficients of greater than 0.98 in adult murine CMs (Figures 3A, 3C, and 3E; Movie S2). We then repeated a similar type of analysis on rod-like hESC-CMs and demonstrated that BASiC-generated cell length curves were highly correlated with manual cell length curves, with Pearson's correlation coefficients of 0.98 (Figures 3B, 3D, and 3E; Movie S1). Importantly, automated edge detection methods could not generate usable contraction curves for hESC-derived CMs because of the relatively low-contrast edges of these cell types, highlighting the need for an automated alternative to edge detection. Similarly, these cells do not have well developed sarcomeres.

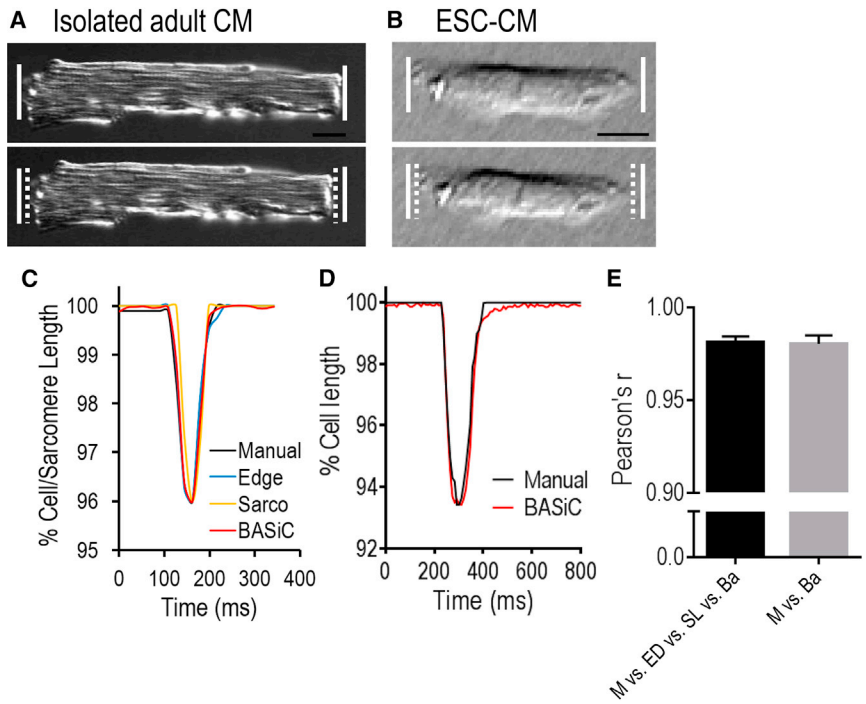

Figure 3. Validation of Contraction Curve in Isolated Adult Murine CMs and hESC-CMs

(A and B) Comparison of representative isolated murine adult CMs (A) and hESC-CMs (B) in a relaxed (top) versus a contracted (bottom) state. Solid white lines represent the position of cell edges in a relaxed state. Dotted white lines represent the position of cell edges in a contracted state. Scale bars, 10 μm.

(C and D) Contraction curves generated by manual measurement (black line), edge detection (blue line), sarcomere length measurement (yellow line), and BASiC (red line) of the representative murine adult CM (C) and the representative hESC-CM (D).

(E) Pearson's correlation coefficient (Pearson's r) between contraction curves generated by manual measurement (M), edge detection (ED), sarcomere length measurement (SL), and BASiC (Ba) of adult CMs (black bar, n = 15 cells from 3 independent experiments) and hESC-CMs (gray bar, n = 16 cells from 3 independent experiments).

Data are represented as mean ± SE. See also Figure S2 and Movies S1 and S2.

In addition, we analyzed the similarity between contraction curves generated by BASiC and manual measurements of irregularly shaped hESC-CMs cultured on PDMS (i.e., non-rod-like), hESC-CM clusters cultured on PDMS or in suspension, and hESC-CM monolayers on polystyrene (Figures S2A–S2I). We found Pearson's correlation coefficients of above 0.95 under all of these conditions, indicating the applicability of BASiC to analyze CM contractility in variable setups. Further testing revealed that differences in frame rate, light intensity, and resolution during image acquisition had a minimal effect on BASiC analysis (Figures S2J–S2O).

Mechanical Model for Quantification of Force Generation

We then sought to quantify the force generated by individual CMs by traction force microscopy (TFM), a well validated methodology used to estimate the force generated by individual CMs (McCain et al., 2014). In traditional TFM, cells are plated on flexible substrates with fluorescent microspheres attached to the surface of the substrate. As cells shorten, they deform the substrate and, with it, move the attached fluorescent microspheres. Because the stiffness of the substrate is known, it is possible to estimate the contractile force required for its deformation from the movement of the fluorescent microspheres. Because cell shortening is not measured directly but, rather, inferred from microsphere movement, this approach relies on the assumption that microsphere movement and cell shortening are directly correlated. To test this underlying assumption, we cultured hESC-CMs on flexible PDMS substrates embedded with fluorescent microspheres. Cell shortening correlated closely with microsphere movement, validating this assumption (Figure S3A; Movie S3). We then calculated the force generated by single contracting rod-like CMs from the microsphere movement (Figures 4A, 4E, and 4F) with standard techniques and obtained results similar to previous reports (Kuo et al., 2012; McCain et al., 2014). An important limitation of standard TFM approaches is the use of fluorescently labeled microspheres, limiting their compatibility for use in conjunction with fluorescence-based physiological assays such as optical mapping of calcium cycling and action potential. To address this limitation and capitalize on the power of our methodology, we utilized a mechanical model based on cell dimensions, cell shortening, and growth substrate properties to calculate the force generated by single contracting myocytes without the use of fluorescent microspheres (described in detail in the Supplemental Experimental Procedures). A direct comparison of both TFM methodologies (with and without microspheres) revealed highly similar force curves with a mean Pearson's correlation coefficient of 0.96 (Figures 4B and 4C). Likewise, the mean difference in peak force was 8.8 $\mu N/mm^2$ (95% limits of agreement, −33.8–16.2 $\mu N/mm^2$; Figure 4D). We then repeated these experiments with irregularly shaped

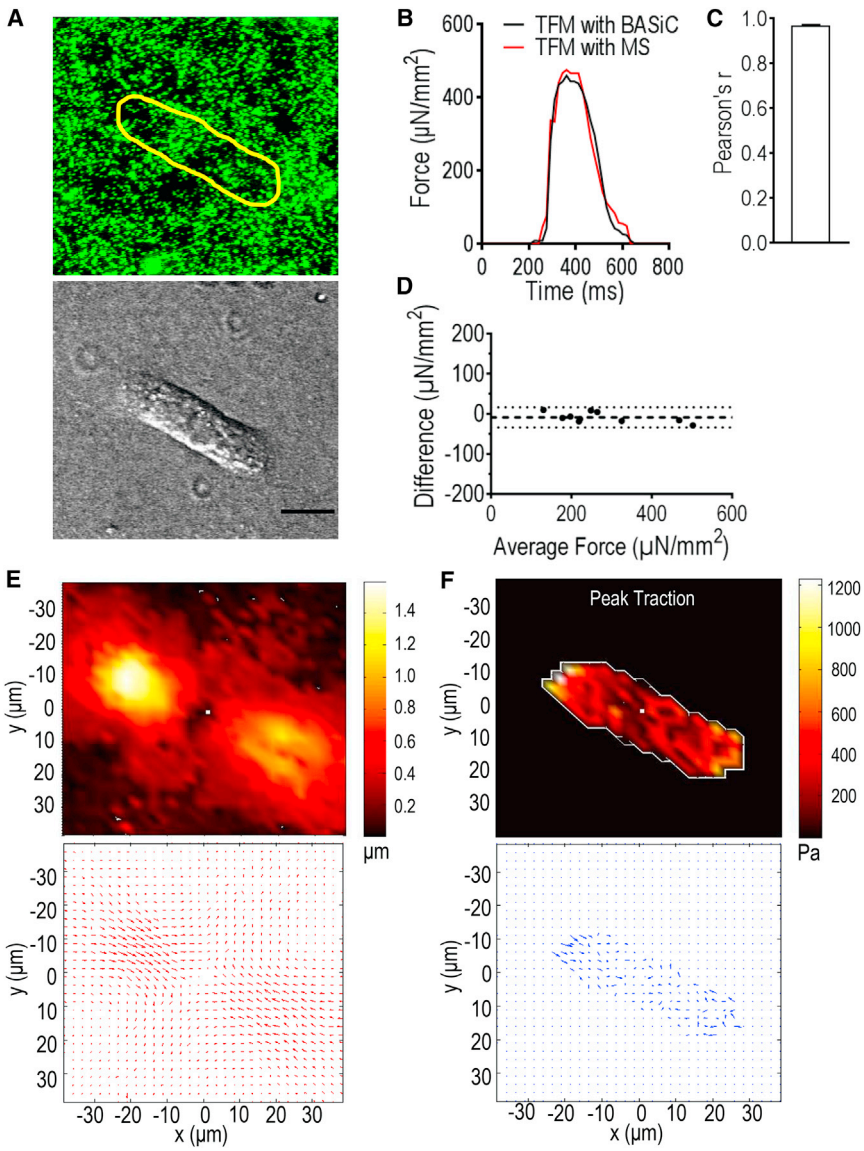

Figure 4. TFM with and without Fluorescent Microspheres for Single-Cell Force Measurement

(A) Top: image of the PDMS surface coated with 200 μM fluorescent microspheres. The yellow outline indicates the outline of the CM at its fully contracted state. Bottom: DIC image of the CM. Scale bar, 10 μm.

(B) Plot of contractile force calculated by TFM using BASiC overlaid with force calculated by TFM using fluorescent microspheres.

(C) Pearson's r between contraction curves generated by the two methods. n = 11 cells from 3 independent experiments.

(D) Bland-Altman graph showing the average of force measured by TFM using BASiC and TFM using fluorescent microspheres plotted against the difference in measurements. The mean difference (dashed line) and 95% limit of agreement (dotted lines) are indicated. n = 10 cells from 3 independent experiments.

(E) Microsphere displacement heatmap (top) and vector map (bottom) of the CM at its peak contraction state compared with its relaxed state.

(F) Traction force heatmap (top) and vector map (bottom) of the CM at its peak contraction compared with its relaxed state. Data are represented as mean ± SE. See also Figure S3 and Movie S3.

hESC-CMs and CM clusters on PDMS and again found highly similar force curves with average Pearson's correlation coefficients of above 0.95. The ratio of peak force calculated by TFM with BASiC over peak force calculated by TFM with microspheres was 1.02 ± 0.04 for CM clusters and 1.40 ± 0.15 for irregularly shaped CMs (Figures S3B–S3G). The correlation in force calculations between TFM with microspheres and BASiC was not affected by the application of the non-selective β-adrenergic agonist isoproterenol (Figures S3H and S3I).

Quantification of Pharmacotherapy Effects

To evaluate the sensitivity of our methodology in detecting small changes in the contractile behavior of individual hESC-CMs, we examined the dose response of two bioactive agents used widely in cardiovascular research. Verapamil is an L-type calcium channel blocker that has been shown to decrease CM contractility (Dolnikov et al., 2006; Turnbull et al., 2014). Conversely, isoproterenol has been shown to increase CM contractility (Brito-Martins et al., 2008). hESC-CMs were paced with field stimulation at a rate of 1.2 Hz, and movies of single rod-like CMs contracting on PDMS gels were captured at baseline and after treatment with 10 and 100 nM of verapamil or isoproterenol. CM contraction curves were then generated as described above. Calcium cycling was also concurrently assessed via fluorescence imaging with the calcium dye Fluo-4 AM. In a control experiment, the effect of Fluo-4 AM on hESC-CM contractility was analyzed over a period of 60 min, and no significant differences in contractility

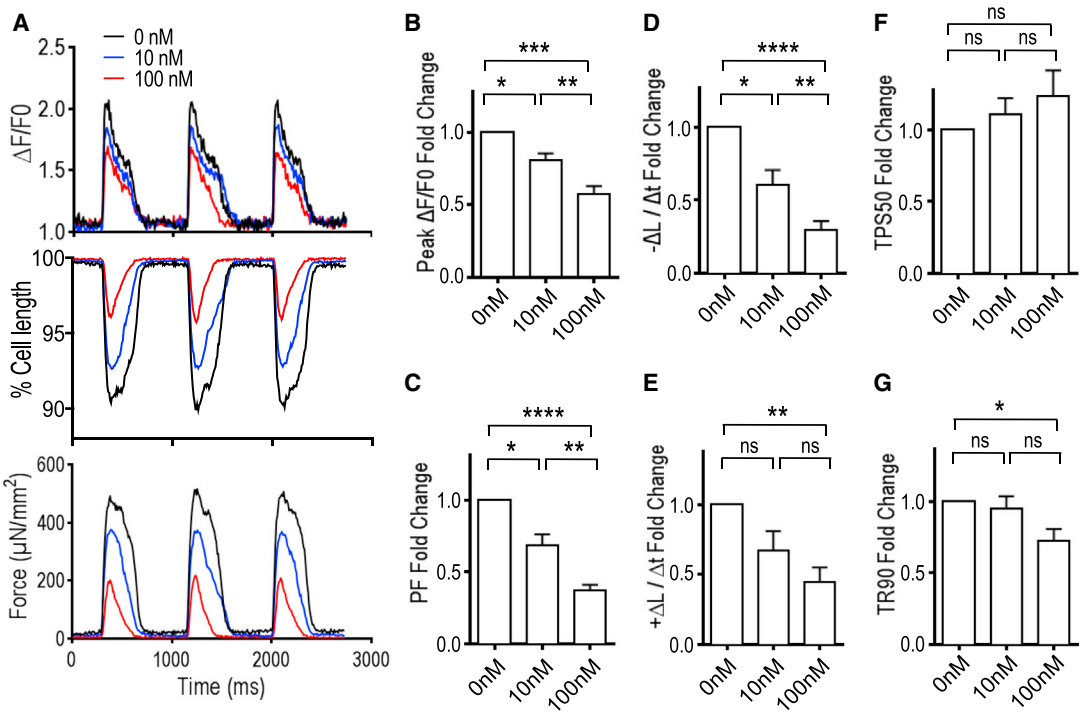

Figure 5. Quantitative Analysis of CM Function in Response to Verapamil

(A) Representative contraction curves of a single field-stimulated hESC-CM treated with the L-type calcium channel blocker verapamil. Changes in Fluo-4 AM calcium transient indicator intensity (top), percentage cell length (center), and contractile force (bottom) of the cell over time are shown.

(B–G) Fold change in calcium transient amplitude (ΔF/F0, B), peak force (PF, C), maximum shortening velocity (−ΔL/Δt, D), maximum relengthening velocity (+ΔL/Δt, E), time to 50% peak shortening (TPS50, F), and time to 90% relengthening (TR90, G) of cells treated with 10 and 100 nM verapamil compared with baseline. n = 8 cells from 3 independent experiments. *p < 0.05; **p < 0.01; ***p < 0.001; ****p < 0.0001; ns, not significant.

Data are represented as mean ± SE. See also Figure S4 and Movie S4.

were found (Figure S4A–S4G). In an additional control experiment with hESC-CMs, the calcium dye intensity remained stable over a period of 60 min (Figure S4H). Treatment with verapamil resulted in decreased contractility and calcium transients, as assessed by fluorescent signal, fractional shortening, and force curves (Figure 5A; Movie S4). Quantitative analysis of the contraction kinetics and calcium cycling revealed negative inotropic and lusitropic effects on CM contractility by the administration of verapamil, with a significant reduction in maximum shortening velocity, peak contractile force, maximum relengthening velocity, and calcium transient amplitude (Figures 5B–5G). In contrast, treatment with isoproterenol resulted in progressive positive inotropic and lusitropic effects with a significant increase in maximum shortening velocity, peak contractile force, and maximum relengthening velocity. We also observed significant decreases in time to 50% peak shortening and time to 90% relengthening (Figure 6). We analyzed the responses to these pharmacological interventions as the average fold change of multiple cells. As expected, because of the heterogeneous nature of hESC-CMs, there was some degree of variability in the functional characteristics of these myocytes at baseline and in response to verapamil (Figure S4I–S4N) and isoproterenol (Figures S5A–S5F). Subsequently, isolated adult mouse CMs field-stimulated at 1 Hz were treated with 100 nM isoproterenol, contraction curves were generated with BASiC, and a significant positive inotropic effect was again observed (Figure S5G–S5M).

Fluorescent transmembrane voltage reporters have been used previously to study toxic electrophysiological changes after treatment with anti-arrhythmic drugs such as dofetilide, a blocker of the rapid component of the delayed rectifier current (IKr). Prior work has demonstrated that dofetilide prolongs the cardiac action potential and can be proarrhythmic at clinically prescribed doses (Leyton-Mange et al., 2014; Roden, 2004). Most studies to date, however, have examined the effect of such drugs exclusively on action potential characteristics (Braam et al., 2010; Leyton-Mange et al., 2014). We hypothesized

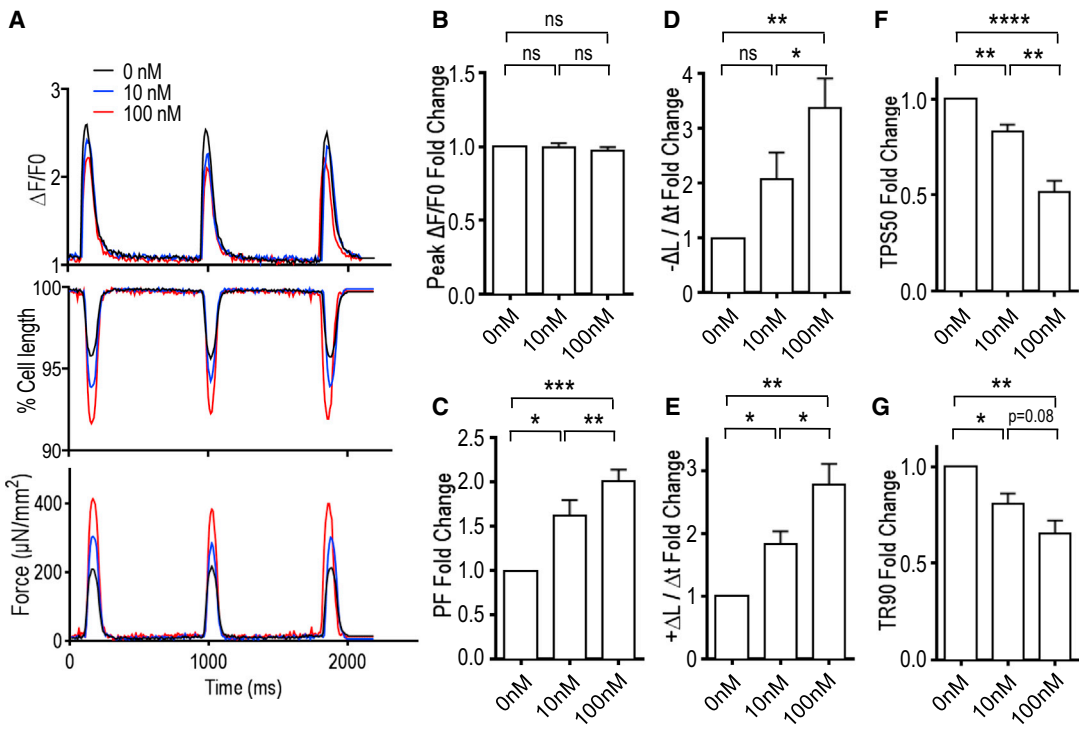

Figure 6. Quantitative Analysis of CM Function in Response to Isoproterenol

(A) Representative contraction curves of a single field-stimulated hESC-CM treated with the β agonist isoproterenol. Changes in Fluo-4 AM calcium transient indicator intensity (top), percentage cell length (center), and contractile force (bottom) of the cell over time are shown. (B–G) Fold change in ΔF/F0 (B), PF (C), −ΔL/Δt (D), +ΔL/Δt (E), TPS50 (F), and TR90 (G) of cells treated with 10 and 100 nM isoproterenol compared with baseline. n = 9 cells from 3 independent experiments. *p < 0.05, **p < 0.01, ***p < 0.001, ****p < 0.0001. Data are represented as mean ± SE. See also Figure S5.

that, by concurrently examining CM contractility and action potential characteristics, we would be able to better assess the cardiotoxicity of such commonly used drugs. Movies of single rod-like CMs contracting on PDMS gels were captured at baseline and after treatment with 10 nM dofetilide. Action potential morphology was concurrently assessed via fluorescence imaging with the transmembrane voltage reporter FluoVolt (Miller et al., 2012). At baseline, hESC-CMs exhibited regular intervals between action potentials and contractions, with consistent peak amplitudes even in the absence of field stimulation (Figure 7A). Upon treatment with the arrhythmogenic agent dofetilide, however, cells exhibited multiple toxic responses, including early afterdepolarizations (Figure 7B; Movie S5), irregular interbeat intervals (IBIs; Figure 7C), and irregular contraction peak amplitudes (PAs; Figure 7D). We then quantified the coefficient of variation (COV) for both the IBI and PA for the cells before and after dofetilide treatment and compared the measurements for the action potential profile and the contractility profile. Although some of the toxic effects were identified in both the action potential and contraction profiles, others were only apparent in the contraction curve, highlighting the need to examine excitation-contraction coupling after treatment with potentially cardiotoxic agents.

DISCUSSION

The advent of human induced pluripotent stem cell technology coupled to advances in directed cardiac differentiation protocols has opened new avenues for the study of human myocardial physiology and pathophysiology. Recent studies have focused on disease-specific human induced PSC-CMs' electrophysiology and calcium cycling properties for cardiac disease modeling or, alternatively, on myocardial contractility (Itzhaki et al., 2011; Lan et al., 2013). To date, the simultaneous assessment of calcium cycling, action potential characteristics, contractile kinetics, and force generation has been challenging. Current methodologies geared at assessing myocardial contractility of adult CMs typically rely on edge detection techniques that directly assess CM shortening (Chen et al., 2014) or the change in sarcomere striations over

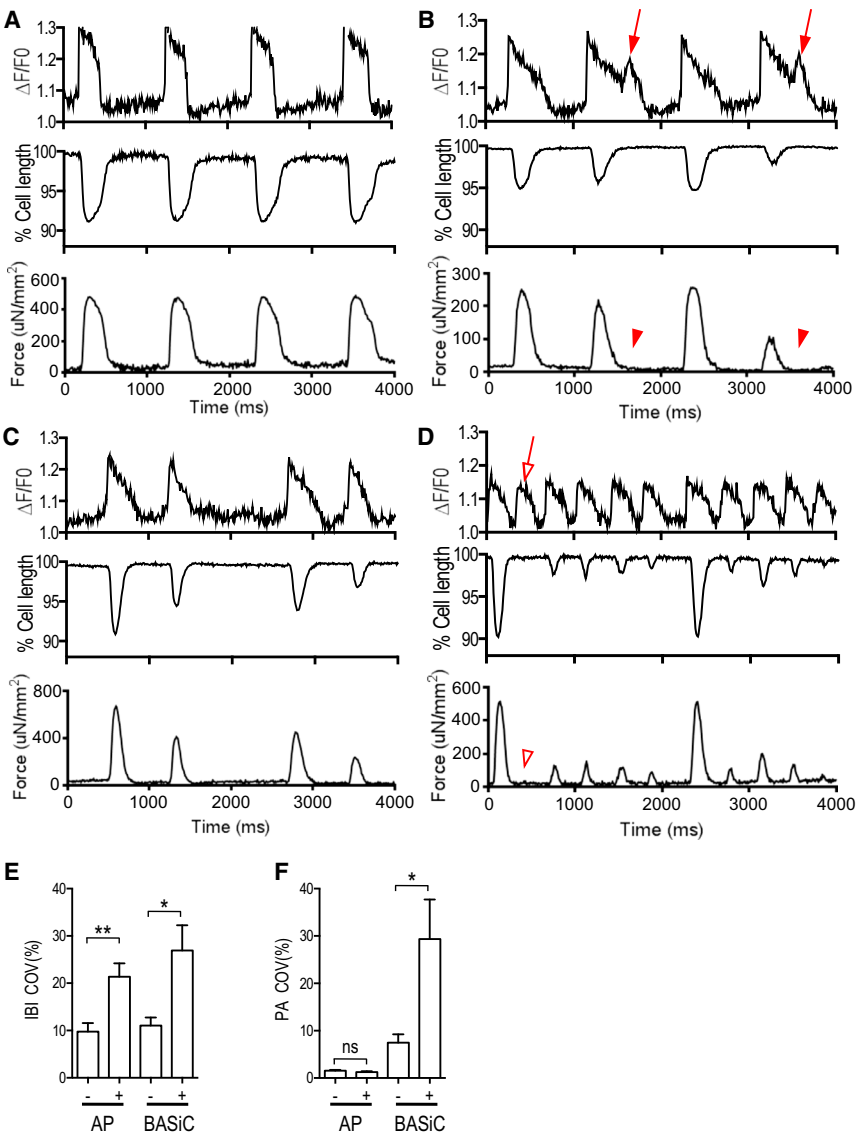

Figure 7. Rapid Evaluation of Drug-Induced Cardiac Toxicity in Single Cardiomyocytes

(A) Representative contraction curves of a single spontaneously contracting CM at baseline (0 nM dofetilide). Changes in FluoVolt action potential indicator intensity (top), percentage cell length (center), and contractile force (bottom) of the cell over time are shown.

(B–D) Representative contraction curves of single CMs treated with 10 nM of dofetilide showing occurrences of early afterdepolarizations (closed arrows) without aftercontractions (closed arrowheads) (B), irregular interbeat intervals (IBIs) and peak contraction amplitudes (PAs) (C), and absent contractions (open arrowheads) with regular action potential (open arrows) in addition to irregular IBIs and PAs (D).

(E) The coefficient of variation (COV) of the IBIs measured by action potential (AP) and BASiC treated with (+) and without (−) dofetilide.

(F) The COV of the PAs measured by AP and BASiC treated with (+) and without (−) dofetilide. *$p < 0.05$, **$p < 0.01$. $n = 10$ cells from 3 independent experiments.

Data are represented as mean ± SE. See also Movie S5.

time (Bub et al., 2010). These approaches require cells with clearly defined cellular borders and distinct striations, limiting their applicability to less mature cell types (Gherghiceanu et al., 2011). Likewise, current TFM approaches for the measurement of contractile force of single myocardial cells require the use of fluorescent microspheres, limiting their capacity for use in conjunction with other fluorescence-based physiological assays. Other approaches, including optical flow analysis, yield a unit-less or dual-peaked curve rather than standard fractional shortening and force generation curves (Ahola et al., 2014; Hayakawa et al., 2014; Maddah et al., 2015).

Here we present a methodology that provides a flexible tool for the study of contraction kinetics of single myocardial cells at different stages of maturation cultured on substrates with tunable stiffness. Our approach is based on comparing the similarity of frames in a movie of CMs contracting on well characterized flexible substrates and yields a standard contraction curve of hPSC-CMs contracting against strain. Critically, this allows the generation of fractional shortening curves and the calculation of contraction and relaxation velocities similar to those used in many studies of adult cardiomyocytes. We then incorporate the mechanical properties of the growth substrate to quantify the kinetics of force generation at single-cell resolution and in myocardial clusters. We demonstrate that our approach is ideally suited for rod-like cells and myocardial clusters and has a high degree of correlation with standard TFM, which requires the use of fluorescent microspheres. Because we do not use fluorescence for the assessment of

force generation, our approach is readily suitable for the concurrent assessment of the kinetics of force generation along with calcium cycling and action potential at single-cell resolution. An important advantage of the simultaneous assessment of force generation and electrophysiological characteristics is the ability to unequivocally determine whether a pathophysiological process results in electromechanical dissociation. Because our approach yields fractional shortening curves, it should also allow an easier comparison of the contractile phenotype between hPSC-CMs and adult CMs in maturation studies, disease modeling, and pharmacological experiments. Importantly, our method is economical and widely applicable because it only requires movie microscopy without the need for highly specialized hardware or genetically engineered cell lines. Although our approach does not currently offer real-time analysis, it can be automated readily to allow for this in the future.

In proof-of-principle experiments, we examined the response of hESC-derived CMs to verapamil and isoproterenol, two drugs commonly used in cardiovascular research. Single CMs exhibited a significantly reduced calcium transient amplitude associated with a negative inotropic response to treatment with the L-type Ca^{2+} channel blocker verapamil. These results are in accordance with previous reports from hPSC-CM-based tissue-engineered heart tissues (Turnbull et al., 2014), embryoid bodies (EBs; Dolnikov et al., 2006), and hPSC-CM monolayers (Himmel, 2013). Likewise, we observed a dose-dependent positive inotropic response to isoproterenol. Prior studies using hPSC-CMs have found a variable inotropic response to isoproterenol. Although some studies show a significant inotropic response in EBs and single hPSC-CMs (Hayakawa et al., 2014; Reppel et al., 2004), other studies show a transient or no response in EBs and engineered heart tissue (Brito-Martins et al., 2008; Turnbull et al., 2014).

Over the past decades, numerous drug development projects have been halted by concerns over cardiotoxicity. Because significant differences exist between humans and rodents, hPSC-CMs have been suggested as a promising alternative to rodent adult CMs. Several studies using hPSC-CMs for cardiotoxicity screening have been performed with different readouts of toxicity, such as increased action potential duration and the occurrence of early afterdepolarizations (Braam et al., 2010; Liang et al., 2013). We demonstrate our ability to rapidly detect drug-induced cardiac toxicity by assessing contractility and action potential simultaneously. Our finding that excitation-contraction coupling may be perturbed under toxic conditions suggests that simultaneously assessing action potential characteristics and contractile behavior may improve the sensitivity of drug-induced cardiac toxicity screening.

The treatment of heart failure represents a major unmet clinical need. Despite the recent advances in regenerative medicine, at this time, drug-based therapy remains the cornerstone of treatment for heart failure. Our methodology should have broad applications in the study of normal and diseased myocardial contractile physiology and should be suitable for drug discovery and toxicology testing using normal or diseased stem cell-derived myocardial cells.

EXPERIMENTAL PROCEDURES

Generation of Flexible Culture Substrates

Flexible substrates were generated by adding 50 μl of Sylgard 527 PDMS, parts A and B mixed at a 1:1 ratio, onto a Fluorodish (WPI) and curing at 60°C for 6 hr.(Palchesko et al., 2012) Subsequently the Fluorodishes were UV-sterilized and coated with Matrigel (BD Biosciences) prior to cell seeding.

Human Embryonic Stem Cell Maintenance and Cardiac Differentiation

hESCs from the lines HUES-9 and HES-3 NKX2-5$^{eGFP/w}$ were cultured with mTESR-1 growth medium (STEMCELL Technologies) in polystyrene plates coated with Matrigel (BD Biosciences) as described previously. Cardiac differentiation of hESCs was performed using a protocol established previously (Lian et al., 2012).

Fluorescence-Activated Cell Sorting

The simultaneous DIC imaging with fluorescent calcium imaging experiment was performed with GFP$^+$ HES-3 NKX2-5$^{eGFP/w}$ cells. Cells were isolated with a fluorescence-activated cell sorting (FACS) protocol as described previously (Elliott et al., 2011).

Dissociation and Plating

Beating CMs were dissociated into single-cell suspensions after 15–20 days of differentiation as described previously (Atmanli et al., 2014). Single hESC-CMs were seeded on Matrigel-coated Fluorodishes at 2,000—6,000 cells/cm^2. Single contracting CMs and CM clusters growing on PDMS substrates for more than 2 weeks were chosen for drug treatment and image acquisition. To obtain hESC-CM clusters in suspension, beating CMs were treated with 0.05% Trypsin (Life Technologies) for 5 min, after which the reaction was neutralized with 10% fetal bovine serum (Life Technologies).

Confocal Imaging and Drug Treatment

Single contracting CMs and CM clusters cultured on flexible substrates, CM clusters in suspension, and CM monolayers on polystyrene were imaged in CM culture medium using a Nikon A1R confocal microscope atop an anti-vibration table (TMC). Cells were placed inside a climate control chamber at 37°C with 5% CO_2 (Pathology Devices) 30 min prior to the start of the experiments. For the verapamil and isoproterenol experiments, the cells were field-stimulated with 10 V at 1.2 Hz using the RC-37WS perfusion insert with electrodes (Warner Instruments) connected to a C-Pace EP stimulator (Ion Optix). Movie recording of

CM contraction cycles was performed using a Nikon A1R confocal microscope with DIC microscopy using a 488- or 647-nm laser. Movies were acquired with at least 100 fps unless described otherwise. Movies of CMs displaying at least five contraction cycles were recorded at baseline and then 5 min after each treatment. Cells were treated with verapamil (Sigma), isoproterenol (Sigma), or dofetilide (Sigma) as described in the Results. For calcium imaging, 0.5 μM of Fluo-4 AM (Life Technologies) was added to the CM culture medium 10 min prior to image acquisition. For action potential imaging, a FluoVolt membrane potential kit (Life Technologies) was used at a dilution of 1:1,000 according to the manufacturer's protocol. Both fluorescence and DIC channels were recorded concurrently for multiple contraction cycles.

Data Analysis and Display

The Nikon Elements software package and Fiji were used for movie file conversions.(Schindelin et al., 2012). Movies were cropped using Fiji to isolate the contracting CM from neighboring cells and cellular debris. Movies were loaded into Visible software (Reify) (Garakani et al., 2015; Drubin et al., 2006; Garakani, 2008; Hack et al., 2004; C.A. MacRae et al., 2005, International Conference on Systems Biology, conference presentation) to generate a similarity matrix of n rows by n columns, where n is the number of frames in the movie. Analysis of the similarity matrix was performed in Excel (Microsoft). For analysis of contraction curves, at least five contraction curves from a single video were averaged by matching the start of the contractions. Curve-fitting was applied to this averaged curve to obtain accurate measurements of maximum shortening and relengthening velocities and time to 50% shortening and 90% relengthening, respectively. The three-dimensional matrices were generated using GNU Octave and MATLAB (MathWorks).

Traction Force Microscopy with Fluorescent Microspheres

We used a well established fluorescent microsphere-based method to calculate the contractile force of CMs (Hazeltine et al., 2012; McCain et al., 2014). Briefly, fluorescent microspheres (Invitrogen) were coated onto PDMS substrates. The substrates were then UV-sterilized and coated with Matrigel (BD Biosciences). CMs were seeded onto the substrates and cultured for 14 days. Movies of single CMs and CM clusters contracting on the substrates were recorded in both fluorescent and DIC channels. The software package TractionForAll (Marinković et al., 2012) was used to analyze images from the movies and calculate the force generated by CMs.

Traction Force Microscopy without Fluorescent Microspheres

Contractile forces generated by shortening CMs were calculated in MATLAB based on the contractility curve generated with BASiC, the dimensions of the CM, and the mechanical properties of the PDMS substrate (Palchesko et al., 2012). Variable input for the MATLAB script is the width of the cell in centimeters, the length of the cell (in the direction of contraction) in centimeters, and the amount of cell shortening in centimeters. The Young's modulus of PDMS substrates was 5 kPa for all experiments. The MATLAB script and related mechanical model are based on several assumptions, described in detail in the Supplemental Experimental Procedures.

Statistical Analysis

All data were analyzed using GraphPad Prism 6 software (GraphPad Software) and presented as means ± SE from the number of cells indicated in the text and figure legends. Raw data were analyzed for normal distribution using the Kolmogorov-Smirnov test. Contraction kinetics and force generation data were compared using repeated-measures ANOVA followed by Bonferroni post-test analysis for multiple comparisons. Coefficient of variation data were compared using paired t test. Force generation data after calculation with two different TFM methods before and after application of isoproterenol were compared using repeated-measures two-way ANOVA. Differences were considered significant at $p < 0.05$.

SUPPLEMENTAL INFORMATION

Supplemental Information includes Supplemental Experimental Procedures, five figures, one table, and eight movies and can be found with this article online at http://dx.doi.org/10.1016/j.stemcr.2015.10.017.

AUTHOR CONTRIBUTIONS

J.D.K. and D.H. designed and performed the experiments reported in Figures 1, 2, 3, 4, 5, 6, and 7 and wrote the manuscript. N.M. and E.K. contributed the mechanical model for force generation calculations. P.V.D.M. mentored colleagues and edited the manuscript. A.G. wrote the Visible software and mentored colleagues. I.J.D. designed experiments, mentored colleagues, and wrote the manuscript.

ACKNOWLEDGMENTS

We thank the Massachusetts General Hospital Program in the Membrane Biology Microscopy Core Facility for contributions to the setup and image acquisition on the Nikon A1R. We thank Reify Corporation for the use of the Visible software. We thank C. Cowan from the Harvard Stem Cell Institute for the generous gift of the HUES-9 cell line and D. Eliot from the Murdoch Children's Research Institute for the generous gift of the HES-3 NKX2-5$^{eGFP/w}$ cell line. We thank Nikita Shah for assistance with the data analysis and isolation of adult murine cardiomyocytes. This work was supported by grants from the NIH/National Heart, Lung, and Blood Institute (U01HL100408-01 and 1K08 HL091209) and a grant from the Dutch Heart Foundation (2013SB013). A.G. is a founder of Reify.

Received: April 2, 2015
Revised: October 28, 2015
Accepted: October 29, 2015
Published: November 25, 2015

REFERENCES

Ahola, A., Kiviaho, A.L., Larsson, K., Honkanen, M., Aalto-Setälä, K., and Hyttinen, J. (2014). Video image-based analysis of single

human induced pluripotent stem cell derived cardiomyocyte beating dynamics using digital image correlation. Biomed. Eng. Online *13*, 39.

Atmanli, A., Hu, D., and Domian, I.J. (2014). Molecular etching: a novel methodology for the generation of complex micropatterned growth surfaces for human cellular assays. Adv. Healthc. Mater. *3*, 1759–1764.

Braam, S.R., Tertoolen, L., van de Stolpe, A., Meyer, T., Passier, R., and Mummery, C.L. (2010). Prediction of drug-induced cardiotoxicity using human embryonic stem cell-derived cardiomyocytes. Stem Cell Res. (Amst.) *4*, 107–116.

Brito-Martins, M., Harding, S.E., and Ali, N.N. (2008). beta(1)- and beta(2)-adrenoceptor responses in cardiomyocytes derived from human embryonic stem cells: comparison with failing and non-failing adult human heart. Br. J. Pharmacol. *153*, 751–759.

Bub, G., Camelliti, P., Bollensdorff, C., Stuckey, D.J., Picton, G., Burton, R.A., Clarke, K., and Kohl, P. (2010). Measurement and analysis of sarcomere length in rat cardiomyocytes in situ and in vitro. Am. J. Physiol. Heart Circ. Physiol. *298*, H1616–H1625.

Chen, S., Zhu, P., Guo, H.M., Solis, R.S., Wang, Y., Ma, Y., Wang, J., Gao, J., Chen, J.M., Ge, Y., et al. (2014). Alpha1 catalytic subunit of AMPK modulates contractile function of cardiomyocytes through phosphorylation of troponin I. Life Sci. *98*, 75–82.

Chong, J.J., Yang, X., Don, C.W., Minami, E., Liu, Y.W., Weyers, J.J., Mahoney, W.M., Van Biber, B., Cook, S.M., Palpant, N.J., et al. (2014). Human embryonic-stem-cell-derived cardiomyocytes regenerate non-human primate hearts. Nature *510*, 273–277.

de Tombe, P.P. (1998). Altered contractile function in heart failure. Cardiovasc. Res. *37*, 367–380.

Dolnikov, K., Shilkrut, M., Zeevi-Levin, N., Gerecht-Nir, S., Amit, M., Danon, A., Itskovitz-Eldor, J., and Binah, O. (2006). Functional properties of human embryonic stem cell-derived cardiomyocytes: intracellular Ca2+ handling and the role of sarcoplasmic reticulum in the contraction. Stem Cells *24*, 236–245.

Drubin, D.A., Garakani, A.M., and Silver, P.A. (2006). Motion as a phenotype: the use of live-cell imaging and machine visual screening to characterize transcription-dependent chromosome dynamics. BMC Cell Biol. *7*, 19.

Elliott, D.A., Braam, S.R., Koutsis, K., Ng, E.S., Jenny, R., Lagerqvist, E.L., Biben, C., Hatzistavrou, T., Hirst, C.E., Yu, Q.C., et al. (2011). NKX2-5(eGFP/w) hESCs for isolation of human cardiac progenitors and cardiomyocytes. Nat. Methods *8*, 1037–1040.

Garakani, A.M. (2008). Discovering Underlying Similarities in Video. In Multimedia Information Extraction: Papers from the AAAI Fall Symposium. http://www.aaai.org/Papers/Symposia/Fall/2008/FS-08-05/FS08-05-013.pdf.

Garakani, A.M., Hack, A.A., Roberts, P., and Walter, S. (2015). Method and apparatus for acquisition, compression, and characterization of spatiotemporal signals. U.S. patent US7672369 B2.

Gherghiceanu, M., Barad, L., Novak, A., Reiter, I., Itskovitz-Eldor, J., Binah, O., and Popescu, L.M. (2011). Cardiomyocytes derived from human embryonic and induced pluripotent stem cells: comparative ultrastructure. J. Cell. Mol. Med. *15*, 2539–2551.

Glick, M.R., Burns, A.H., and Reddy, W.J. (1974). Dispersion and isolation of beating cells from adult rat heart. Anal. Biochem. *61*, 32–42.

Hack, A.A., Ahouse, J., Roberts, P.G., and Garakani, A.M. (2004). New methods for automated phenotyping of complex cellular behaviors. Conf. Proc. IEEE Eng. Med. Biol. Soc. *7*, 5124–5126.

Hayakawa, T., Kunihiro, T., Ando, T., Kobayashi, S., Matsui, E., Yada, H., Kanda, Y., Kurokawa, J., and Furukawa, T. (2014). Image-based evaluation of contraction-relaxation kinetics of human-induced pluripotent stem cell-derived cardiomyocytes: Correlation and complementarity with extracellular electrophysiology. J. Mol. Cell. Cardiol. *77*, 178–191.

Hazeltine, L.B., Simmons, C.S., Salick, M.R., Lian, X., Badur, M.G., Han, W., Delgado, S.M., Wakatsuki, T., Crone, W.C., Pruitt, B.L., and Palecek, S.P. (2012). Effects of substrate mechanics on contractility of cardiomyocytes generated from human pluripotent stem cells. Int. J. Cell Biol. *2012*, 508294.

Himmel, H.M. (2013). Drug-induced functional cardiotoxicity screening in stem cell-derived human and mouse cardiomyocytes: effects of reference compounds. J. Pharmacol. Toxicol. Methods *68*, 97–111.

Itzhaki, I., Maizels, L., Huber, I., Zwi-Dantsis, L., Caspi, O., Winterstern, A., Feldman, O., Gepstein, A., Arbel, G., Hammerman, H., et al. (2011). Modelling the long QT syndrome with induced pluripotent stem cells. Nature *471*, 225–229.

Kuo, P.L., Lee, H., Bray, M.A., Geisse, N.A., Huang, Y.T., Adams, W.J., Sheehy, S.P., and Parker, K.K. (2012). Myocyte shape regulates lateral registry of sarcomeres and contractility. Am. J. Pathol. *181*, 2030–2037.

Lan, F., Lee, A.S., Liang, P., Sanchez-Freire, V., Nguyen, P.K., Wang, L., Han, L., Yen, M., Wang, Y., Sun, N., et al. (2013). Abnormal calcium handling properties underlie familial hypertrophic cardiomyopathy pathology in patient-specific induced pluripotent stem cells. Cell Stem Cell *12*, 101–113.

Leyton-Mange, J.S., Mills, R.W., Macri, V.S., Jang, M.Y., Butte, F.N., Ellinor, P.T., and Milan, D.J. (2014). Rapid cellular phenotyping of human pluripotent stem cell-derived cardiomyocytes using a genetically encoded fluorescent voltage sensor. Stem Cell Reports *2*, 163–170.

Lian, X., Hsiao, C., Wilson, G., Zhu, K., Hazeltine, L.B., Azarin, S.M., Raval, K.K., Zhang, J., Kamp, T.J., and Palecek, S.P. (2012). Robust cardiomyocyte differentiation from human pluripotent stem cells via temporal modulation of canonical Wnt signaling. Proc. Natl. Acad. Sci. USA *109*, E1848–E1857.

Liang, P., Lan, F., Lee, A.S., Gong, T., Sanchez-Freire, V., Wang, Y., Diecke, S., Sallam, K., Knowles, J.W., Wang, P.J., et al. (2013). Drug screening using a library of human induced pluripotent stem cell-derived cardiomyocytes reveals disease-specific patterns of cardiotoxicity. Circulation *127*, 1677–1691.

Liu, J., Sun, N., Bruce, M.A., Wu, J.C., and Butte, M.J. (2012). Atomic force mechanobiology of pluripotent stem cell-derived cardiomyocytes. PLoS ONE *7*, e37559.

Maddah, M., Heidmann, J.D., Mandegar, M.A., Walker, C.D., Bolouki, S., Conklin, B.R., and Loewke, K.E. (2015). A non-invasive platform for functional characterization of stem-cell-derived

cardiomyocytes with applications in cardiotoxicity testing. Stem Cell Reports *4*, 621–631.

Marinković, A., Mih, J.D., Park, J.A., Liu, F., and Tschumperlin, D.J. (2012). Improved throughput traction microscopy reveals pivotal role for matrix stiffness in fibroblast contractility and TGF-β responsiveness. Am. J. Physiol. Lung Cell. Mol. Physiol. *303*, L169–L180.

McCain, M.L., Yuan, H., Pasqualini, F.S., Campbell, P.H., and Parker, K.K. (2014). Matrix elasticity regulates the optimal cardiac myocyte shape for contractility. Am. J. Physiol. Heart Circ. Physiol. *306*, H1525–H1539.

Miller, E.W., Lin, J.Y., Frady, E.P., Steinbach, P.A., Kristan, W.B., Jr., and Tsien, R.Y. (2012). Optically monitoring voltage in neurons by photo-induced electron transfer through molecular wires. Proc. Natl. Acad. Sci. USA *109*, 2114–2119.

Narula, J., Hajjar, R.J., and Dec, G.W. (1998). Apoptosis in the failing heart. Cardiol. Clin. *16*, 691–710, ix.

Palchesko, R.N., Zhang, L., Sun, Y., and Feinberg, A.W. (2012). Development of polydimethylsiloxane substrates with tunable elastic modulus to study cell mechanobiology in muscle and nerve. PLoS ONE *7*, e51499.

Reppel, M., Boettinger, C., and Hescheler, J. (2004). Beta-adrenergic and muscarinic modulation of human embryonic stem cell-derived cardiomyocytes. Cell. Physiol. Biochem. *14*, 187–196.

Roden, D.M. (2004). Drug-induced prolongation of the QT interval. N. Engl. J. Med. *350*, 1013–1022.

Rodriguez, M.L., Graham, B.T., Pabon, L.M., Han, S.J., Murry, C.E., and Sniadecki, N.J. (2014). Measuring the contractile forces of human induced pluripotent stem cell-derived cardiomyocytes with arrays of microposts. J. Biomech. Eng. *136*, 051005.

Schindelin, J., Arganda-Carreras, I., Frise, E., Kaynig, V., Longair, M., Pietzsch, T., Preibisch, S., Rueden, C., Saalfeld, S., Schmid, B., et al. (2012). Fiji: an open-source platform for biological-image analysis. Nat. Methods *9*, 676–682.

Sun, N., Yazawa, M., Liu, J., Han, L., Sanchez-Freire, V., Abilez, O.J., Navarrete, E.G., Hu, S., Wang, L., Lee, A., et al. (2012). Patient-specific induced pluripotent stem cells as a model for familial dilated cardiomyopathy. Sci. Transl. Med. *4*, 130ra47.

Turnbull, I.C., Karakikes, I., Serrao, G.W., Backeris, P., Lee, J.J., Xie, C., Senyei, G., Gordon, R.E., Li, R.A., Akar, F.G., et al. (2014). Advancing functional engineered cardiac tissues toward a preclinical model of human myocardium. FASEB J. *28*, 644–654.

Yang, X., Pabon, L., and Murry, C.E. (2014). Engineering adolescence: maturation of human pluripotent stem cell-derived cardiomyocytes. Circ. Res. *114*, 511–523.

Zimmermann, W.H., Melnychenko, I., Wasmeier, G., Didié, M., Naito, H., Nixdorff, U., Hess, A., Budinsky, L., Brune, K., Michaelis, B., et al. (2006). Engineered heart tissue grafts improve systolic and diastolic function in infarcted rat hearts. Nat. Med. *12*, 452–458.

Stem Cell Reports, Volume *5*

Supplemental Information

Integrated Analysis of Contractile Kinetics, Force Generation, and Electrical Activity in Single Human Stem Cell-Derived Cardiomyocytes

Jan David Kijlstra, Dongjian Hu, Nikhil Mittal, Eduardo Kausel, Peter van der Meer, Arman Garakani, and Ibrahim J. Domian

Supplemental Figures

Figure S1

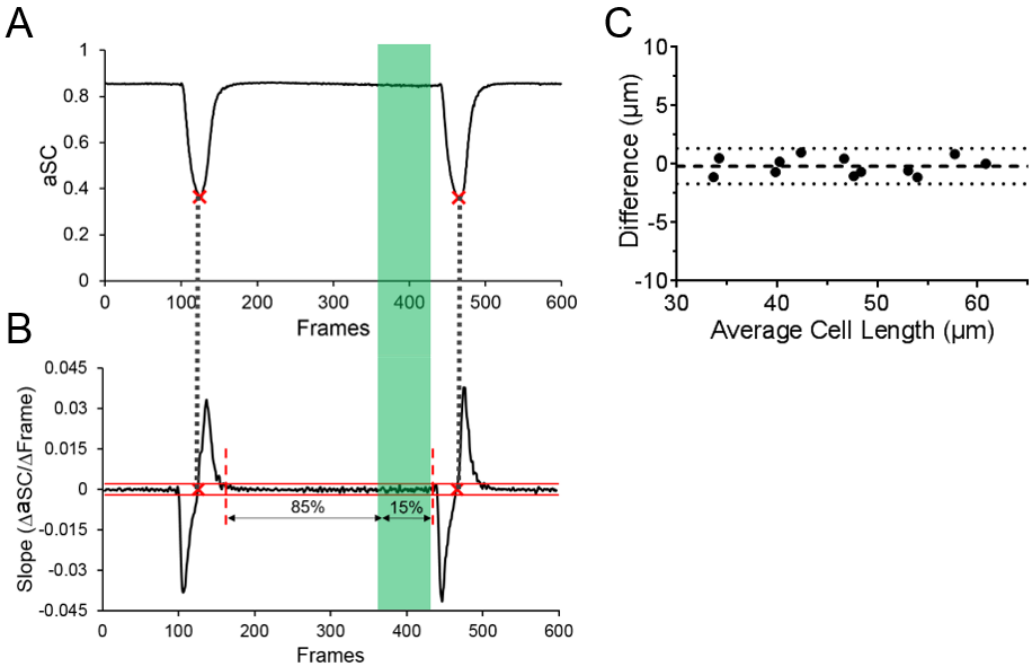

Figure S1. Selection of Pre-contractile Frames and Reliability of Cell Length Measurements, Related to Figure 2. (**A**) Graph of averaged SC (aSC) of all frames over frame number for Movie S1. Red crosses mark the points of maximum contraction (local minimum). (**B**) Slope (ΔaSC/ΔFrame) of the rolling five-point linear fit line. The inter-contractile interval is marked by dashed red lines and defined as frames with a deviation of slope from 0 of less than 5% of the minimum slope as indicated by red lines. Frames in the terminal 15% of the inter-contractile interval are defined as pre-contractile marked by the green shaded area. The dotted black lines show the correlation between maximum contraction points in aSC and slope. (**C**) Bland-Altman graph of average cell length measurement of two observers plotted against the difference between measurements. Cell length measurements between observers were highly similar with a mean difference (dashed line) of 0.17µm (not significantly different from 0; P = 0.45) and 95% limits of agreement (dotted lines) of -1.69µm to 1.35µm. n = 12 cells from 3 independent experiments.

Figure S2

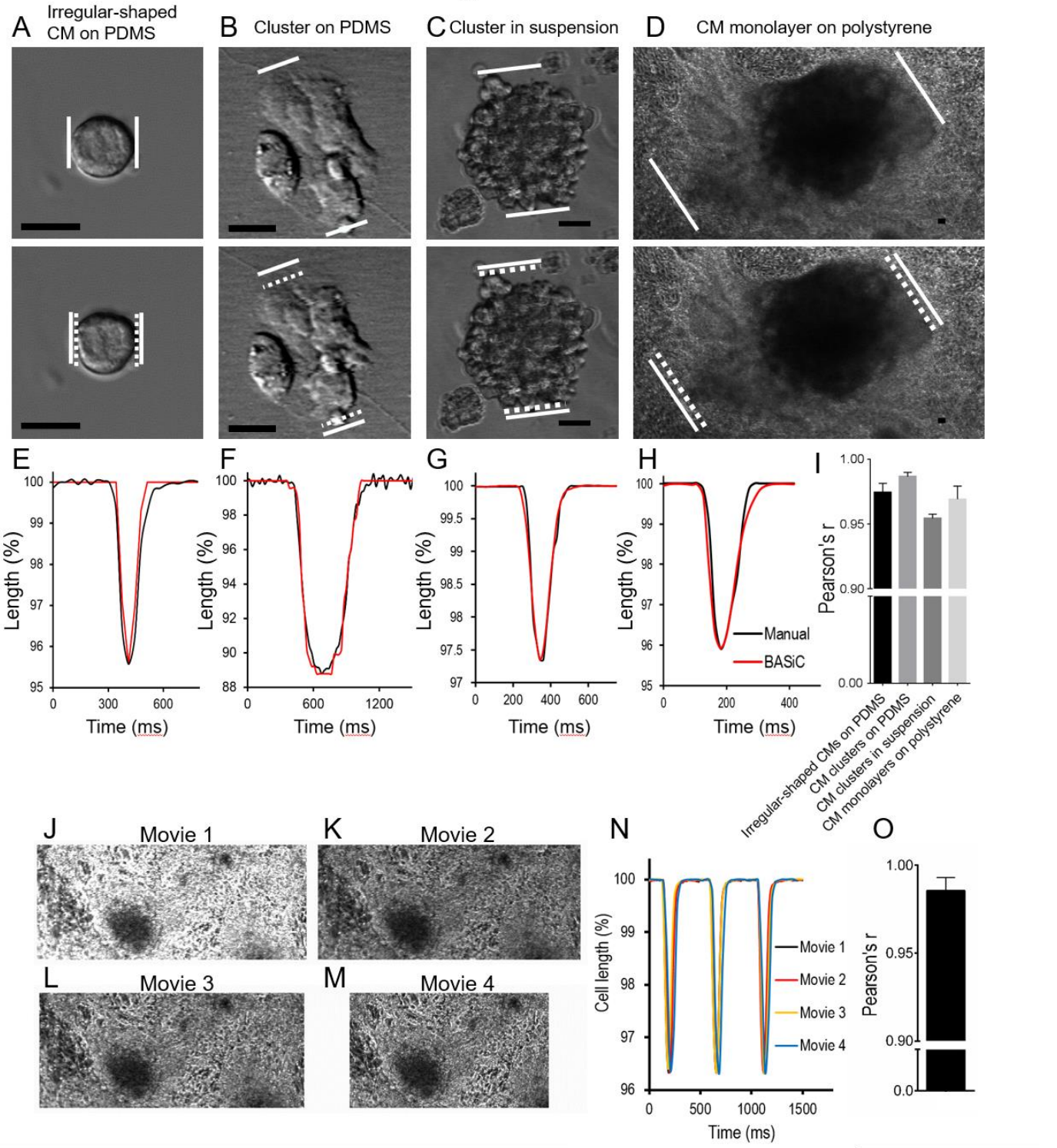

Figure S2. Validation of BASiC for Irregular-shaped CMs, CM Clusters, and Monolayers and Different Movie Acquisition Settings, Related to Figure 3. (A-D) Comparison of a representative irregular shaped hESC-CM on PDMS, hESC-CM cluster on PDMS, hESC-CM cluster in suspension and hESC-CM monolayer on polystyrene in a relaxed (top panel) vs. a contracted (bottom panel) state. Solid white lines represent position of cell structure edges in relaxed state. Dotted white lines represent position of cell structure edges in contracted state. Scale bars, 20 µm. **(E-H)** Contraction curves generated by manual measurement (black line), and BASiC (red line) of the representative cell/cluster/monolayer. **(I)** Pearson's correlation coefficient (Pearson's r) between contraction curves generated by manual measurement and BASiC of cells/clusters/monolayers. n= at least 6 from 3 independent experiments for all groups. Data are represented as mean ± SE. **(J-M)** Four movies of the same hESC-CM monolayer on polystyrene acquired with a variety of settings for frame rate, resolution and pixel saturation. Movie 1: 100 fps, resolution 2.52 µm/px, oversaturated lighting. Movie 2: 100 fps, resolution 2.52 µm/px, normal lighting. Movie 3: 55 fps, resolution 2.52 µm/px, normal lighting. Movie 4: 30 fps, resolution 1.26 µm/px and normal lighting. (**N**) Contraction curves generated by BASiC of Movies 1-4 acquired under different settings show a high degree of similarity. (**O**) Pearson's r between contraction curves of movies of hESC-CM monolayers acquired with a variety of settings as described above. n = 5 from 3 independent experiments. Data is represented as mean ± SE. See also Movies S6, S7 and S8.

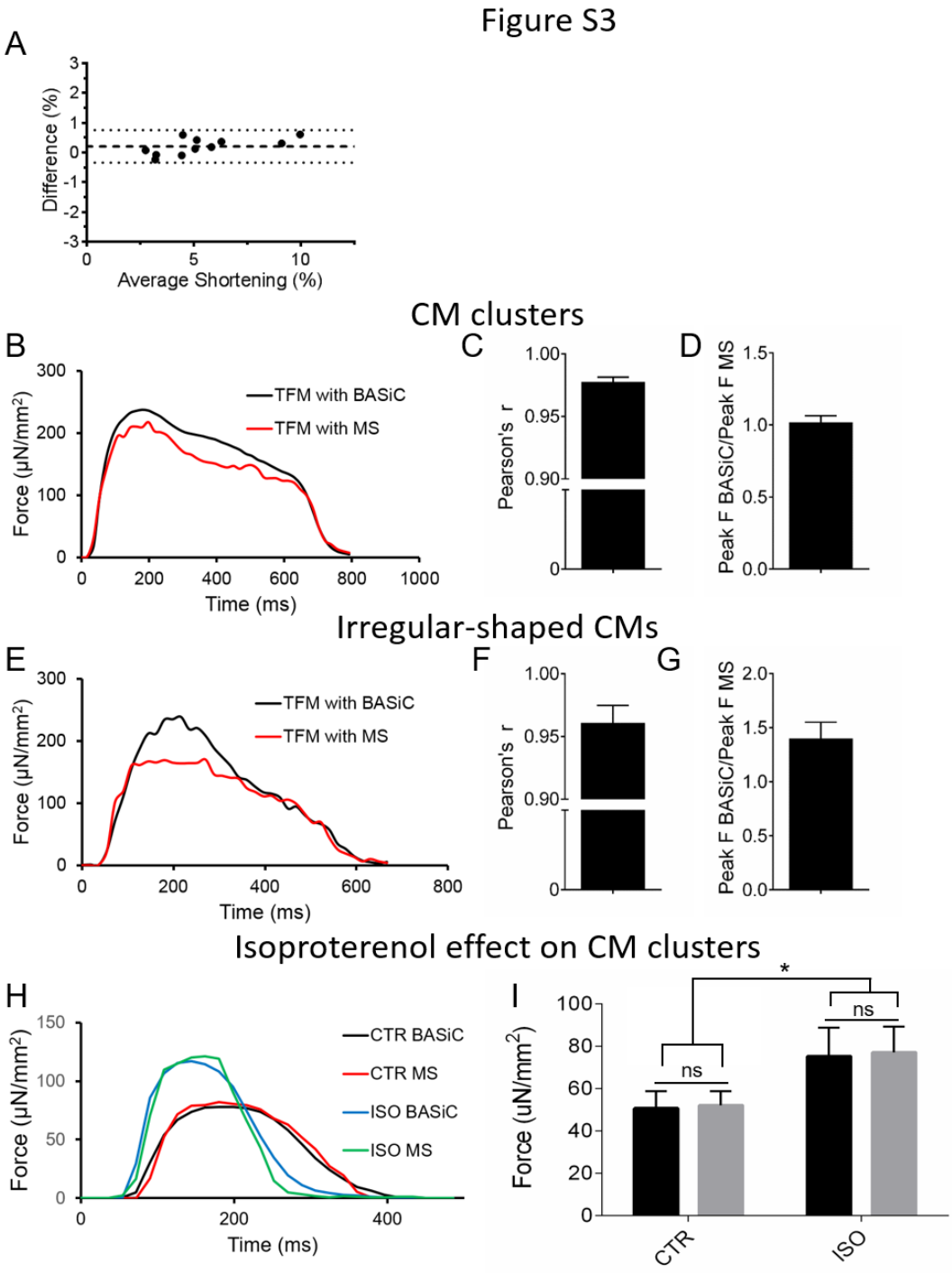

Figure S3. Correlation of Bead Movement and Cell Movement, Force Calculations for CM Clusters and Irregular-shaped CMs, and Isoproterenol Effect on CM Clusters, Related to Figure 4. (**A**) Fluorescent microsphere movement accurately translates into CM shortening. Bland-Altman graph of average of microsphere movement measurement and CM shortening measurement. Microsphere movement and CM shortening correlate closely with a mean difference (dashed line) of 0.16% (not significantly different from 0; P = 0.08) and 95% limits of agreement (dotted lines) of -0.35% to 0.68%. n = 11 cells from 3 independent experiments. (**B**) Plot of contractile force of a hESC-CM cluster calculated by Traction Force Microscopy (TFM) using BASiC overlaid with force calculated by TFM using fluorescent microspheres (MS). (**C**) Pearson's r between contraction curves generated by the two methods. n = 11 CM clusters from 3 independent experiments. (**D**) Ratio of peak force calculated by TFM with BASiC over peak force calculated by TFM with MS. (**E**) Plot of contractile force of a hESC-CM cluster calculated by TFM using BASiC overlaid with force calculated by TFM using MS. (**F**) Pearson's r between contraction curves generated by the two methods. n = 6 cells from 3 independent experiments. (**G**) Ratio of peak force calculated by TFM with BASiC over peak force calculated by TFM with MS. (**H**) Plot of contractile force of a hESC-CM cluster calculated by TFM using BASiC overlaid with force calculated by TFM using fluorescent microspheres (MS) before (CTR) and after (ISO) application of 100nM isoproterenol. (**I**) Average force as calculated by TFM with BASiC and MS before and after application of ISO shows no significant differences between the two methods before and after pharmacological intervention. n = 7 CM clusters from 3 independent experiments. *P<0.05. Data are represented as mean ± SE.

Figure S4

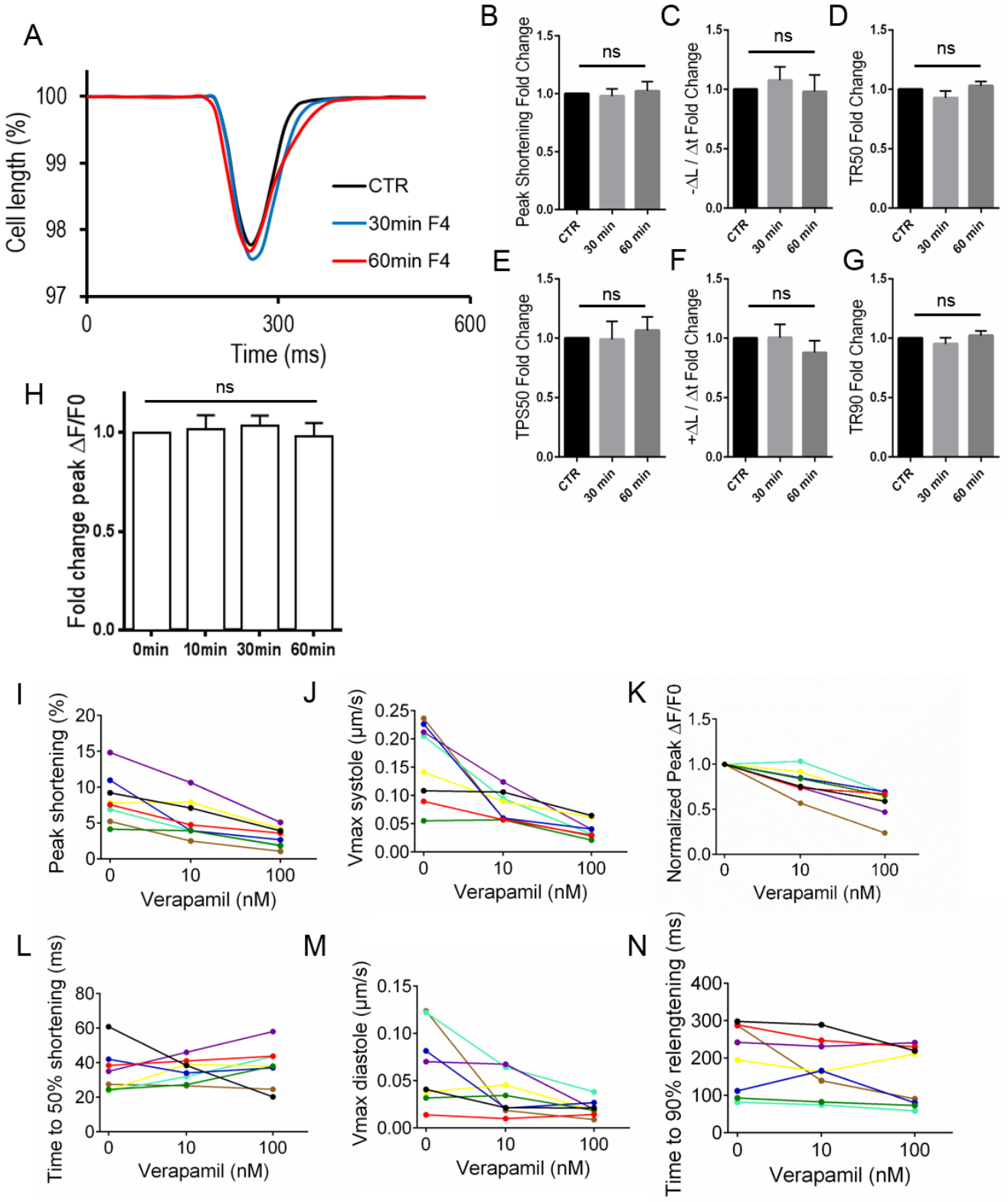

Figure S4. Fluo-4AM Effect and Signal Consistency, and Intercell Variability in Response to Verapamil, Related to Figure 5. (**A**) Representative contraction curves of a single hESC-CM before treatment and 30 min and 60 min after treatment with 0.5µM Fluo-4AM (F4) calcium transient indicator. (**B-G**) Fold change in peak shortening, time to 50% peak shortening (TPS50), maximum shortening velocity (-ΔL/Δt), maximum relengthening velocity (+ΔL/Δt), time to 50% relengthening (TR50) and time to 90% relengthening (TR90) of cells 30 min and 60 min after treatment with 0.5µM Fluo-4AM compared to baseline. n= 6 cells from 3 independent experiments. (**H**) Fold change in peak intracellular fluorescence signal of hESC-CMs loaded with 0.5µM Fluo-4AM. Measurements were taken at 0, 10, 30 and 60 minutes. n= 10 cells from 3 independent experiments. Data are represented as mean ± SE. (**I-N**) Intercellular variability in contractile characteristics of hESC-CMs at baseline and in response to treatment with 10nM and 100nM verapamil. Each colored line represents one cell.

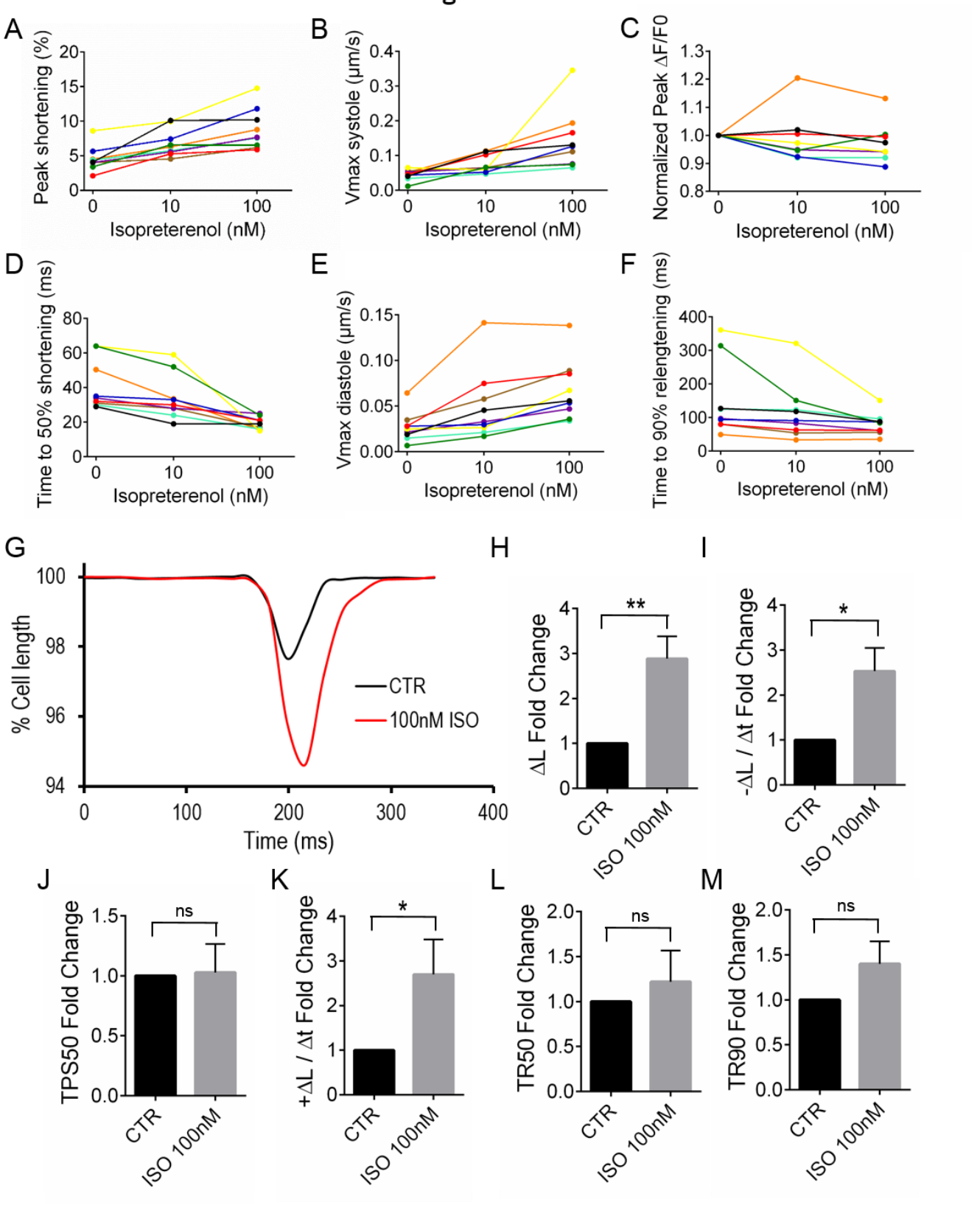

Figure S5. Intercell Variability of hESC-CMs in Response to Isoproterenol and Effect of Isoproterenol on Adult CMs, Related to Figure 6. (**A-F**) Intercellular variability in contractile characteristics of hESC-CMs at baseline and in response to treatment with 10nM and 100nM isoproterenol. Each colored line represents one cell. (**G**) Representative contraction curves of a single isolated field-stimulated adult CM before and after treatment with 100nM isoproterenol. (**H-M**) Fold change in peak shortening (ΔL), maximum shortening velocity (-ΔL/Δt), time to 50% peak shortening (TPS50), maximum relengthening velocity (+ΔL/Δt), time to 50% relengthening (TR50) and time to 90% relengthening (TR90) of adult CMs after treatment with 100nM isoproterenol compared to baseline. n = 7 cells from 3 independent experiments. Data are represented as mean ± SE. *P<0.05; **P<0.01.

Supplemental Experimental Procedures

Normalization of Contraction Curve

The baseline adjusted similarity comparison (BASiC) index and frame numbers of the BASiC contraction curve were normalized to respectively percentage of maximum cell length and time. For this purpose, manual cell length measurements were performed in Fiji(Schindelin et al., 2012) over the longitudinal axis of the cell at the last frame prior to contraction ($length_{max}$) and the peak shortening frame ($length_{min}$). These manual measurements were used in the following equation to normalize BASiC to cell length:

$$Length = length_{max}\ (1 - \frac{1 - SC/SC_{max}}{NR})$$

The SC_{max} was defined as the average SC of the previously selected pre-contractile frames. SC_{min} is the SC value at the peak shortening frame. The Normalization Ratio (NR) is a measure of the relative change in SC compared to the relative change in length during a contraction and is defined as:

$$NR = \frac{1 - SC_{min}/SC_{max}}{1 - length_{min}/length_{max}}$$

Traction Force Microscopy without Fluorescent Microspheres

To calculate contractile force generated by cardiomyocytes on flexible substrates with a static mechanical model we make the following assumptions: 1.) The cell is rectangular, and contracts along one of its directions, without any lateral impediment. 2.) The stiffness of the cell is negligible compared to the stiffness of the gel to which the cell is attached. 3.) The shearing forces are symmetric with respect to the center, that is, they point in opposite directions and cancel in the aggregate. 4.) The shearing traction distribution is assumed to be governed by Boussinesq's law $\sim 1/\sqrt{1-\left(\frac{x}{a}\right)^2}$, where a is the half-length of the cell.

For the 5kPa PDMS used in these experiments the Poisson's ratio (ν) was set to 0.5, the mass density of the gel (ρ) was set to 1.08 g/cm^3, and the shear wave velocity (C_s) was set to 200.8 cm/s. The shear modulus (G) was then calculated as:

$G = \rho C_s^2$

We sub-divide the rectangular cell of dimensions $2a \times 2b$ into narrow rectangles of width Δx . Consider a rectangular load of dimension $\Delta x \times 2b$ and magnitude q_x applied at the free surface of the half-space, with its sides oriented parallel to the x, y axes. It can be shown that the horizontal displacement at the center of the load is given by

$$u_{ox} = \frac{2q_x}{\pi G}\{I_1(\frac{1}{2}\Delta x, b) + \nu[I_2(\frac{1}{2}\Delta x, b) - I_1(\frac{1}{2}\Delta x, b)]\},$$

Where

$$I_1(a,b) = \tfrac{1}{2}\int_0^{2b}\int_0^{2a} \frac{dx\,dy}{\left(x^2+y^2\right)^{1/2}} = a\,\sinh^{-1}\frac{b}{a} + b\,\sinh^{-1}\frac{a}{b}$$

$$I_2(a,b) = \tfrac{1}{2}\int_0^{2b}\int_0^{2a} \frac{x^2 dx\,dy}{\left(x^2+y^2\right)^{3/2}} = b\sinh^{-1}\frac{a}{b},$$

We consider next the case of contact stresses underneath the cardiomyocyte that follow the Boussinesq law:

$$q_x = \frac{2bq_0}{\sqrt{1-\left(\frac{x}{a}\right)^2}}$$

The displacement elicited by each narrow slit at any location is then evaluated via equation (1), scaling the intensity q_0 of the load so that the total elongation of the cell equals the cell's length (i.e. unit strain). Finally, the force needed to accomplish that strain is computed as

$$P_x = q_0\,2b\int_0^a \frac{1}{\sqrt{1-\left(\frac{x}{a}\right)^2}}dx = \pi q_0 ab\,.$$

Isolation of Adult Mouse Cardiomyocytes

Mouse hearts from adult C57BL/6 mice were perfused with a Langendorff apparatus as previously reported(Graham et al., 2013). Briefly, a 12-gauge mouse feeding needle was inserted into the aorta and the heart was subsequently perfused for 18 min at a rate of 1 ml min^{-1} with Tyrode Buffer supplemented with 5.5 mM D-(+)-Glucose (Sigma), 5mM Taurine (Sigma), 10 mM 2,3-Butanedione monoxime (Sigma), 0.5 mg ml^{-1} collagenase A (Roche) and 0.5 mg ml^{-1} collagenase B (Roche) at 37°C. Next, the heart was minced with micro dissecting forceps to dissociate the tissue into single CMs. The cell solution was transferred to Tyrode Buffer supplemented with 1.2 mM CaCl (Sigma) and 5.5 mM D-(+)-Glucose (Sigma) and placed in a Fluorodish for imaging as described above. Rod-like single cells paced at 1 Hz with sharply defined membranes were selected for imaging. All animal care and experimental procedures were approved by the Massachusetts General Hospital Institutional Animal Care and Use Committee.

Edge Detection

Edge detection was performed by plotting a line intensity profile over the longitudinal axis of the CM in Fiji (Schindelin et al., 2012) where the edge contrast for both the left and right edge was optimal, similar to commonly used edge detection software (Fang et al., 2008). The cell edge was defined as the location of the mean of the maximum and minimum intensity value in the high contrast region of the line profile at the cell edge. The cell length over time was subsequently determined by calculating the distance between the location of the left and right edge of the cell in each frame of a movie.

Sarcomere Length Measurement

Sarcomere length measurement was performed by plotting a line intensity profile in Fiji (Schindelin et al., 2012) over the longitudinal axis of the CM to cover at least 10 sarcomeres, similar to commonly used sarcomere length measurement software (Bub et al., 2010). Due to the alternating dark and light A- and I-bands, the line intensity profile had a sinusoidal appearance. The distance between at least 10 peaks was divided by the number of peaks to reflect the average sarcomere length.

Supplemental References

Bub, G., Camelliti, P., Bollensdorff, C., Stuckey, D.J., Picton, G., Burton, R.A., Clarke, K., and Kohl, P. (2010). Measurement and analysis of sarcomere length in rat cardiomyocytes in situ and in vitro. Am J Physiol Heart Circ Physiol *298*, H1616-1625.

Fang, C.X., Dong, F., Thomas, D.P., Ma, H., He, L., and Ren, J. (2008). Hypertrophic cardiomyopathy in high-fat diet-induced obesity: role of suppression of forkhead transcription factor and atrophy gene transcription. American journal of physiology Heart and circulatory physiology *295*, H1206-H1215.

Graham, E.L., Balla, C., Franchino, H., Melman, Y., del Monte, F., and Das, S. (2013). Isolation, culture, and functional characterization of adult mouse cardiomyoctyes. Journal of visualized experiments : JoVE, e50289.

Schindelin, J., Arganda-Carreras, I., Frise, E., Kaynig, V., Longair, M., Pietzsch, T., Preibisch, S., Rueden, C., Saalfeld, S., Schmid, B., *et al.* (2012). Fiji: an open-source platform for biological-image analysis. Nature methods *9*, 676-682.